ACS APPLIED MATERIALS & INTERFACES

www.acsami.org

Research Article

Impact of Nanoparticle Physicochemical Properties on Protein Corona and Macrophage Polarization

Baixue Xiao, Yuxuan Liu, Indika Chandrasiri, Clyde Overby, and Danielle S. W. Benoit*

Cite This: *ACS Appl. Mater. Interfaces* 2023, 15, 13993−14004

Read Online

ACCESS | Metrics & More | Article Recommendations | Supporting Information

ABSTRACT: Macrophages, the major component of the mononuclear phagocyte system, uptake and clear systemically administered nanoparticles (NPs). Therefore, leveraging macrophages as a druggable target may be advantageous to enhance NP-mediated drug delivery. Despite many studies focused on NP−cell interactions, NP-mediated macrophage polarization mechanisms are still poorly understood. This work aimed to explore the effect of NP physicochemical parameters (size and charge) on macrophage polarization. Upon exposure to biological fluids, proteins rapidly adsorb to NPs and form protein coronas. To this end, we hypothesized that NP protein coronas govern NP−macrophage interactions, uptake, and subsequent macrophage polarization. To test this hypothesis, model polystyrene NPs with various charges and sizes, as well as NPs relevant to drug delivery, were utilized. Data suggest that cationic NPs potentiate both M1 and M2 macrophage markers, while anionic NPs promote M1-to-M2 polarization. Additionally, anionic polystyrene nanoparticles (APNs) of 50 nm exhibit the greatest influence on M2 polarization. Proteomics was pursued to further understand the effect of NPs physicochemical parameters on protein corona, which revealed unique protein patterns based on NP charge and size. Several proteins impacting M1 and M2 macrophage polarization were identified within cationic polystyrene nanoparticles (CPNs) corona, while APNs corona included fewer M1 but more M2-promoting proteins. Nevertheless, size impacts protein corona abundance but not identities. Altogether, protein corona identities varied based on NP surface charge and correlated to dramatic differences in macrophage polarization. In contrast, NP size differentially impacts macrophage polarization, which is dominated by NP uptake level rather than protein corona. In this work, specific corona proteins were identified as a function of NP physicochemical properties. These proteins are correlated to specific macrophage polarization programs and may provide design principles for developing macrophage-mediated NP drug delivery systems.

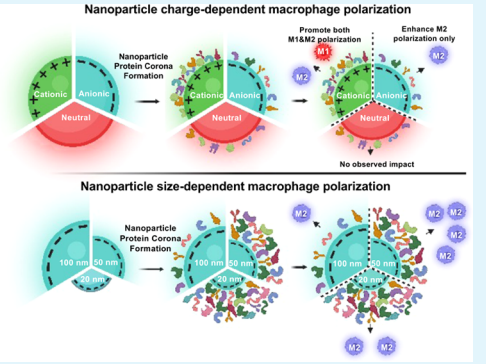

KEYWORDS: *nanoparticles, drug delivery, protein corona, macrophage polarization, surface charge, nanoparticle size*

INTRODUCTION

Nanoparticle (NP)-based drug delivery systems (DDSs) have been widely investigated for myriad applications.[1−5] Despite this investment, most systemically administered NPs are taken up and eliminated by the mononuclear phagocyte system (MPS), one of the significant barriers to DDS translation into effective therapies.[6−8] As a critical cellular component of MPS, leveraging macrophages as a druggable target may be advantageous to enhance DDS delivery.[9−12] Macrophages are actively involved in many diseases, where various macrophage polarization statuses and types, such as classically activated macrophage (M1 macrophage) and alternatively activated macrophage (M2 macrophage) phenotypes, exert significant differences in disease progression. M1 macrophages, which secrete pro-inflammatory cytokines, are upregulated in aged and diabetic patients, leading to delayed fracture healing or even failed healing.[13] In addition, M2 macrophages are less effective for tissue repair in these chronic inflammatory conditions.[13,14] Therefore, in this context, promoting M2 macrophage polarization and/or inhibiting M1 macrophage differentiation may enhance healing. In contrast, anti-inflammatory M2 macrophages support tumor growth and metastasis.[11,15,16] Tumor-associated macrophages (TAMs) share many common features with M2 macrophages, leading to suppression of anti-tumor immune reactivity, one of the current limitations of cancer therapies.[11,15,17−19] Hence, suppressing M2 and elevating M1 macrophage polarization may improve treatment outcomes for various diseases or injuries.

NPs with different physicochemical properties differentially affect macrophage polarization.[20] Specifically, NPs made from silica, gold, carbon, and other metals promote M1 polarization, while polymeric and liposomal NPs tend to induce M2

Received: December 13, 2022
Accepted: February 22, 2023
Published: March 14, 2023

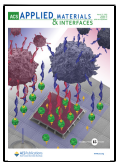

https://doi.org/10.1021/acsami.2c22471
ACS Appl. Mater. Interfaces 2023, 15, 13993−14004

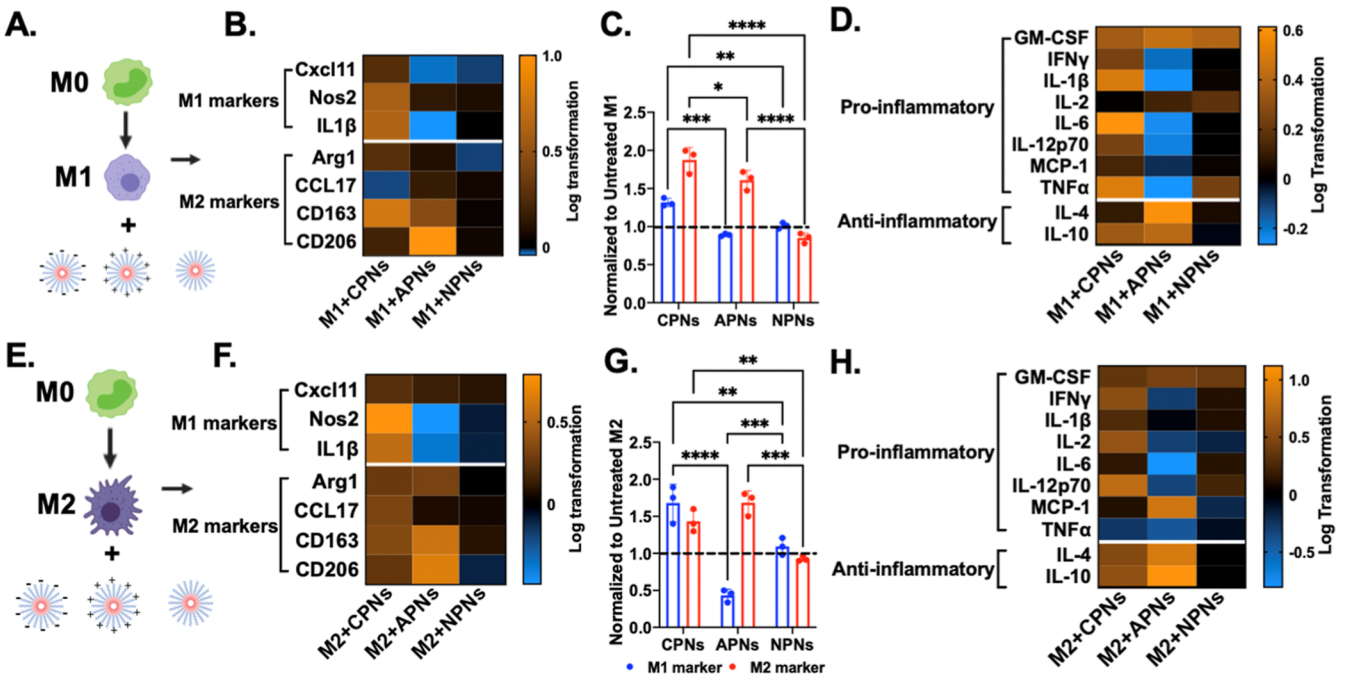

Figure 1. Model anionic, cationic, and neutral nanoparticles composed of polystyrene (APNs, CPNs, and NPNs) suggest charge-dependent macrophage polarization. (A,E) Schematic of primary mouse macrophage polarization. (B,F) Heatmap of all tested genes represented as the log-transformed normalized data (normalized to the housekeeping gene, GAPDH, as well as untreated M1, and M2, respectively), showed both upregulation of M1 and M2 genes after CPN treatment while elevated M2 but downregulation of the M1 gene after APN treatment. A similar trend was found using flow cytometry (C,G) of the expression of the M1 macrophage differentiation markers, MHCII, and CD38, and M2 markers, CD206, and CD163. Data represented as mean ± standard deviation (SD), $n = 3$. ***$p < 0.001$, ****$p < 0.0001$, compared to untreated controls as determined by one-way ANOVA. (D,H) Heatmaps of all tested inflammatory cytokines represented as log-transformed normalized data (normalized to untreated M1 and M2, respectively) suggested increased pro-inflammatory and anti-inflammatory cytokines after CPN treatment. In contrast, after APN treatment, there is downregulation of pro-inflammatory cytokines and but upregulation of anti-inflammatory factors.

macrophage polarization.[10,21] However, these findings are inconsistent. For example, anionic epoxide-modified poly(*N*-isopropylacrylamide-*co*-acrylic acid) [p(NIPAm-*co*-AAc)] NPs promoted macrophage M2 polarization,[22] while anionic carboxyl-modified polystyrene NPs upregulated M1 markers as well as pro-inflammatory cytokine expression.[23] Despite numerous studies, the underlying mechanism of NP-mediated macrophage polarization is still not fully understood.[20]

Upon introduction to biological fluids, proteins rapidly adsorb onto NPs and form protein coronas, providing the NP−protein corona as a new biologically active entity.[24−27] Therefore, the protein corona drives NP−macrophage interactions and subsequent macrophage uptake and polarization.[28−31] Physicochemical characteristics, such as NP material, size, and surface properties, have been suggested to play a role in determining the protein corona profile,[24,32−34] which may alter NP−macrophage interactions and downstream polarization. Several studies have investigated the impact of NP protein corona on macrophage uptake. Indeed, NP charge and hydrophobicity affect protein corona formation and macrophage uptake.[35,36] Furthermore, protein corona formation is controlled by the hydrophobicity and bulkiness of chemical moieties utilized to modify NPs, which directly affects the uptake of NPs by macrophages.[35,36] Additionally, Walkey et al. investigated the impact of NP size and poly(ethylene glycol) (PEG) grafting density on NP protein adsorption and macrophage uptake.[37] However, this study focused on tuning NP design to minimize macrophage uptake rather than studying macrophage polarization. Although it has been considered that NP−cell interaction and subsequent cellular response (uptake, translocation, and function) are closely related to protein adsorption,[10,20,22,24,38−40] the impact of NP protein corona on macrophage polarization is poorly understood. One study demonstrated that the corona formed on AuNP is dynamic, leading to variable macrophage polarization as a function of incubation times.[41] However, investigation of the underlying mechanism governing the link between protein corona and macrophage polarization was inconclusive. Altogether, the importance of macrophages and protein coronas highlights the need for a comprehensive and fundamental understanding of how NP physicochemical properties affect protein corona formation and macrophage polarization.

This work evaluated the impact of NP charge and size on macrophage polarization, comprehensively characterized the protein corona profiles from these NPs, and established foundational knowledge on the underlying mechanism of how NP physicochemical properties influence macrophage polarization via the protein corona. First, model polystyrene NPs with various charges and sizes were used to study the impact of NPs on bone marrow-derived macrophages. Gene expression, cell surface markers, and released cytokines were evaluated to characterize macrophage polarization. After incubation with serum, the protein corona was analyzed using proteomics to determine the quantity and identity of proteins and their impact on macrophage polarization. Three NP systems previously developed for various delivery applications were also explored to compare these findings to NPs more relevant to drug delivery. This study sought to understand the effect of NP physicochemical properties on macrophage polarization

https://doi.org/10.1021/acsami.2c22471
ACS Appl. Mater. Interfaces 2023, 15, 13993−14004

Table 1. Characterization of NP Physicochemical Properties

polymer[a]							NP[b]		
	block 1		block 2		diblock copolymer				
name	name/repeats	Mn (kDa)	name/repeats	Mn (kDa)	Mn (kDa)	PDI	size (nm)	PDI	ζ potential (mV)
DMAEMA-NP	DMAEMA	14.9	DMAEMA-*co*-BMA-*co*-PAA	15.0	29.9	1.04	27 ± 2	0.11	20 ± 1
PSMA-PS-NP	PSMA	20.5	PS	31.0	51.5	1.03	32 ± 3	0.10	−29 ± 2
PEG-PS-NP	PEG	20.0	PS	24.2	42.2	1.05	26 ± 2	0.26	−0.03 ± 0.05

[a]Characterization polymer via NMR (proton nuclear magnetic resonance spectroscopy), GPC (gel permeation chromatography for molecular weights (Mn) and polydispersity index (PDI)). [b]NP characterization via DLS using a Malvern Zetasizer Nano ZS. Values are mean ± SD from three independent experiments.

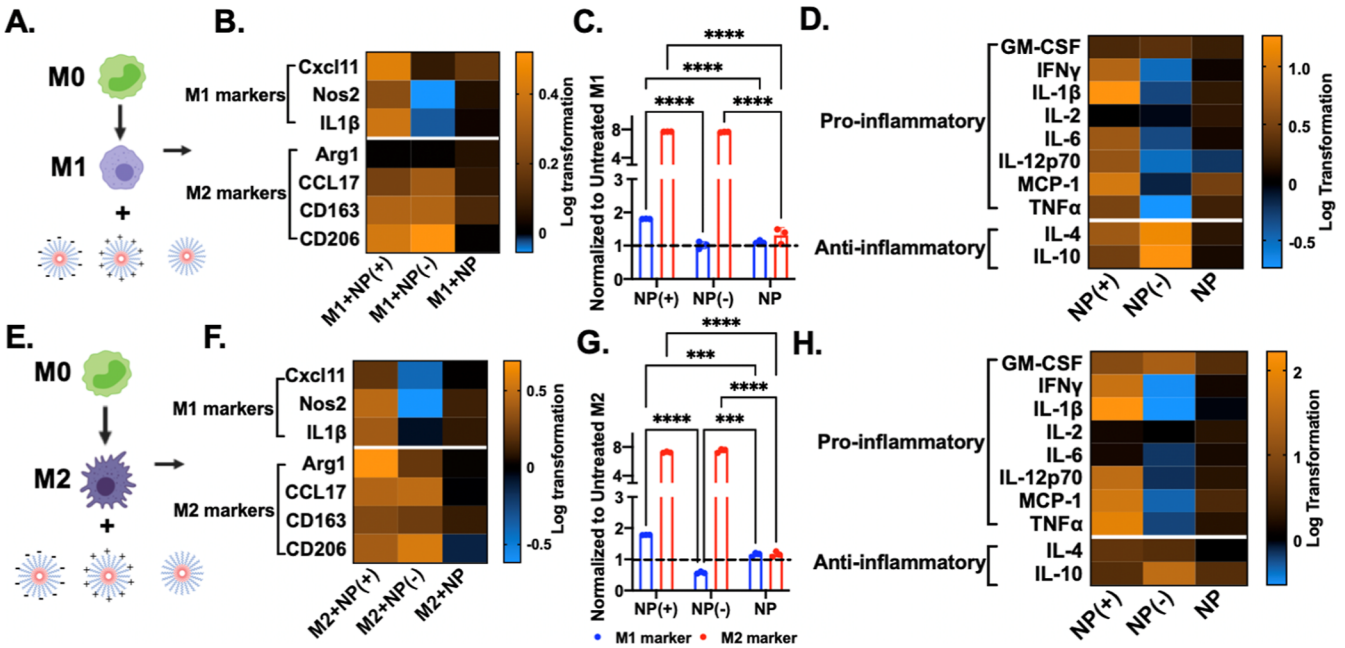

Figure 2. Macrophages treated with cationic nanoparticles [DMAEMA NPs, or NP (+)], anionic nanoparticles [PSMA-PS NPs, or NP (−)], and neutral nanoparticles (PEG-PS NPs, or NP) also exhibited charge-dependent polarization. (A,E) Schematic of primary mouse macrophage polarization. (B,F) Heatmap of all tested genes represented as the log-transformed normalized data (normalized to the housekeeping gene, GAPDH, as well as untreated M1, and M2, respectively) also suggested upregulation of both M1 and M2 genes after cationic NPs treatment, while for anionic nanoparticles, M1 genes were downregulated and M2 genes were promoted. The same trend was shown in flow cytometric analysis (C,G) (M1 macrophage differentiation markers, MHCII and CD38, and M2 markers, CD206 and CD163). Data represented as mean ± SD, $n = 3$. ***$p < 0.001$, ****$p < 0.0001$, compared to untreated controls as determined by one-way ANOVA. (D,H) Heatmap of all tested inflammatory cytokines represented as the log-transformed normalized data (normalized to untreated M1, and M2, respectively).

and how protein coronas associated with NP characteristics guide and modulate macrophage polarization.

RESULTS AND DISCUSSION

In NP DDS design, significant effort has been made to minimize macrophage uptake to improve drug delivery efficiency. Macrophages are ubiquitous cells responsible for the uptake and elimination of NPs[7,20] and can be leveraged as a druggable target to enhance drug delivery efficiency. Interestingly, NPs significantly modulate macrophage polarization, as demonstrated in a few recent studies.[20,37] However, the focus has been on investigating the impact of NPs on macrophage uptake and polarization rather than the underlying mechanisms.[31,35,37,42,43] Numerous properties, such as NP composition, size, shape, and surface modifications, affect the responses of cells, including macrophages. Although it has been demonstrated that surface-modified polymeric microparticles can modulate macrophage activity in vivo[22] and that surface modification impacts the interactions between NPs and macrophages,[42] it is unclear how NP physicochemical properties affect macrophage polarization. To address this deficit, we sought to characterize the impact of NP physicochemical properties on macrophage polarization.

To first investigate the impact of NP charge on macrophage polarization, 100 nm polystyrene NPs (Magsphere Inc.) were utilized with cationic (cationic polystyrene NPs, CPNs), anionic (anionic polystyrene NPs, APNs), and neutral (neutral polystyrene NPs, NPNs) surface charges. Initially, the cytocompatibility of polystyrene NPs was analyzed[44] using the macrophage cell line Raw 264.7. As measured using AlamarBlue, a metabolic activity assay, viability was >98% for all NP-treated groups, suggesting that all NPs are cytocompatible (Figure S4). To determine how macrophages respond to the NP surface charge, bone marrow-derived monocytes (BMDMs) were differentiated for 7 days using M-CSF (macrophage colony-stimulating factor) to M0 macrophages, which were then polarized to M1 or M2 macrophages, respectively (see the detailed experiment setup in Figure S4). Macrophage phenotypes, including M0, M1, and M2 macrophages, were treated with CPNs, APNs, or NPNs. To

https://doi.org/10.1021/acsami.2c22471
ACS Appl. Mater. Interfaces 2023, 15, 13993−14004

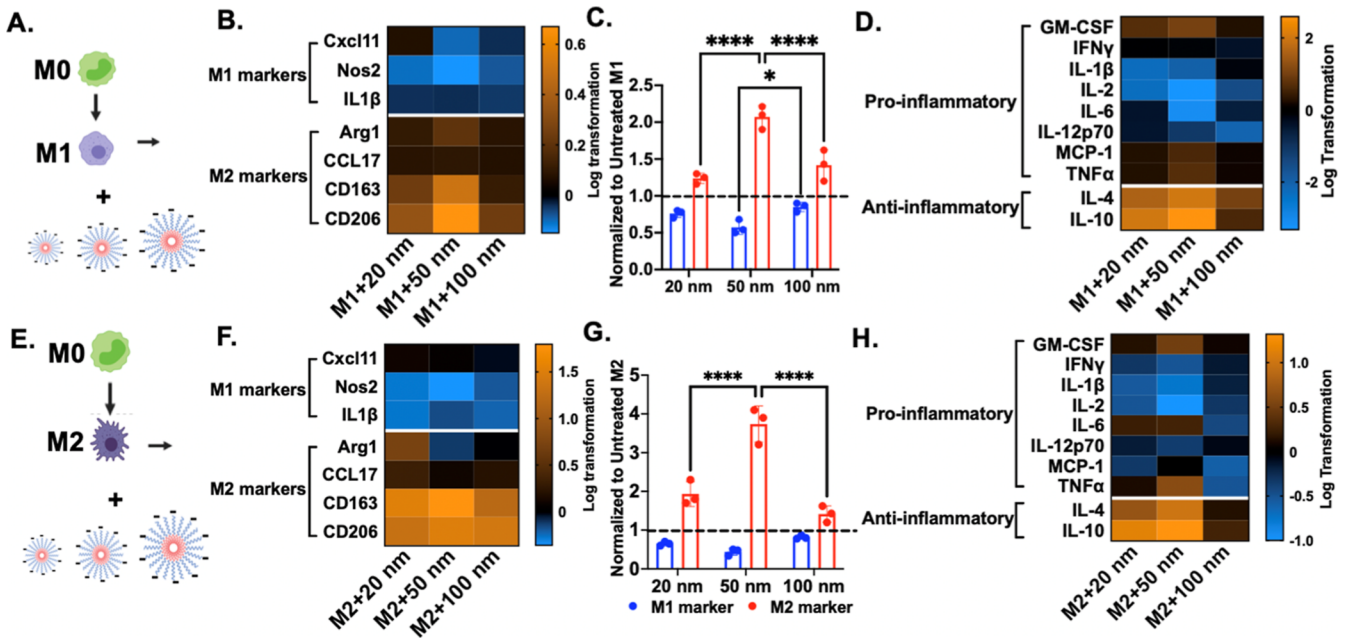

Figure 3. Macrophage polarization is NP size-dependent. (A,E) Schematic of primary mouse macrophage polarization. (B,F) Heatmap of all tested genes represented as the log-transformed normalized data (normalized to a housekeeping gene, GAPDH, as well as untreated M1 and M2, respectively) showed downregulation of M1 genes while upregulation of M2 genes. Among them, 50 nm NPs demonstrated the greatest macrophage modulation. A similar trend was observed in flow cytometric analysis (C,G) of the expression of the M1 macrophage differentiation markers, MHCII and CD38, and M2 markers, CD206 and CD163. Data represented as mean ± SD, $n = 3$. ***$p < 0.001$, ****$p < 0.0001$, compared to untreated controls as determined by one-way ANOVA. (D,H) Heatmap of all tested inflammatory cytokines represented as the log-transformed normalized data (normalized to untreated M1 and M2, respectively).

characterize macrophage polarization, gene expression and surface marker expression were then evaluated. As indicated in Figure 1, all M1 genes (Cxcl11, Nos2, and IL1β) and the majority of M2 genes (Arg1, CD163, and CD206) were upregulated after CPN treatment. Consistent with qPCR gene expression results, flow cytometry also suggests increases in M2 surface markers (CD206+/CD163+) and upregulation of M1 markers (MHCII+/CD38+). However, after incubation with APNs, downregulation of M1 (Cxcl11, Nos2, and IL1b) and upregulation of M2 genes (Arg1, CCL17, CD163, and CD206) were observed from qPCR analysis, while flow cytometry indicates a ∼1.5-fold decrease of M1 surface markers and ∼2-fold increase of M2 surface markers. Interestingly, neither M1 nor M2 markers changed after NPN treatment.

To further evaluate the NP charge-dependent impact on macrophage polarization, secreted proteins were analyzed. Specifically, cell culture supernatants were collected after NP treatment for 3 days and analyzed using the Mouse Cytokine Proinflammatory Focused 10-Plex Discovery Assay Array (MDF10) (Eve Technologies). As is shown in Figure 1C, compared with untreated M1 macrophages, CPNs elevated both pro-inflammatory (GM-CSF, IFNγ, IL1β, IL-6, IL-12p70, MCP-1, and TNFα) and anti-inflammatory cytokines (IL-4 and IL-10), while APNs reduced pro-inflammatory cytokines (IFNγ, IL1β, IL-6, IL-12p70, and TNFα) and promoted anti-inflammatory cytokines (IL-4 and IL-10). It is worth noting that, consistent with gene level and surface protein level evaluations, no changes in cytokines were observed due to NPN treatment. In sum, the results suggest that CPNs promote M1 macrophage polarization from either M1 or M2 phenotypes, while APNs promote M1-to-M2 modulation, and NPNs have no impact on macrophage polarization.

To investigate whether polystyrene NP charge-dependent macrophage polarization is consistent with NPs more relevant to drug delivery, three NP-based DDSs with varying charges were investigated.[45−47] Specifically, cationic, anionic, and neutral NPs were formed through self-assembly of poly(dimethylaminoethyl methacrylate)-*b*-poly(dimethylaminoethyl methacrylate-*co*-butyl methacrylate-*co*-propylacrylic acid) (p(DMAEMA)-*b*-p(DMAEMA-*co*-BMA-*co*-PAA) or DMAEMA-NP), poly(styrene-*alt*-maleic anhydride)-poly(styrene) (PSMA-PS NP), and poly(ethylene glycol)-*b*-poly(styrene) (PEG-PS NP), respectively. The characteristics of both polymers and NPs via GPC (Figure S2), nuclear magnetic resonance (NMR) (Figure S1), dynamic light scattering (DLS) (Figure S3), and ζ potential measurement are summarized in Table 1, revealing that all NPs had expected surface charges based on surface functionality (20 mV for DMAEMA NP, −26 mV for PSMA-PS NP, and −0.03 mV for PEG-PS NP), as well as consistent sizes of ∼30 nm (Table 1). According to the macrophage polarization data in Figure 2, cationic DMAEMA NPs induce both M1- and M2-polarization simultaneously across different phenotypes, while anionic PSMA-PS NPs promote M2 polarization and inhibit M1 differentiation. These findings agree with current reports on the impact of NP charge on macrophage polarization but to a greater extent (∼8-fold) in M2 marker upregulation for both treated M1 and M2 macrophages. Furthermore, macrophages treated with CPNs secrete higher levels of IL-1 and formed more inflammasomes.[48] In another study, exposing macrophages to cationic polymers such as polyethyleneimine (PEI) stimulates M1-like polarization via toll-like receptor 4 (TLR4) signaling and immune cell infiltration into tumors.[49] The synthetic cationic peptide IDR-1018 drives M1-to-M2 differentiation, enhancing anti-inflammatory activities while main-

https://doi.org/10.1021/acsami.2c22471
ACS Appl. Mater. Interfaces 2023, 15, 13993−14004

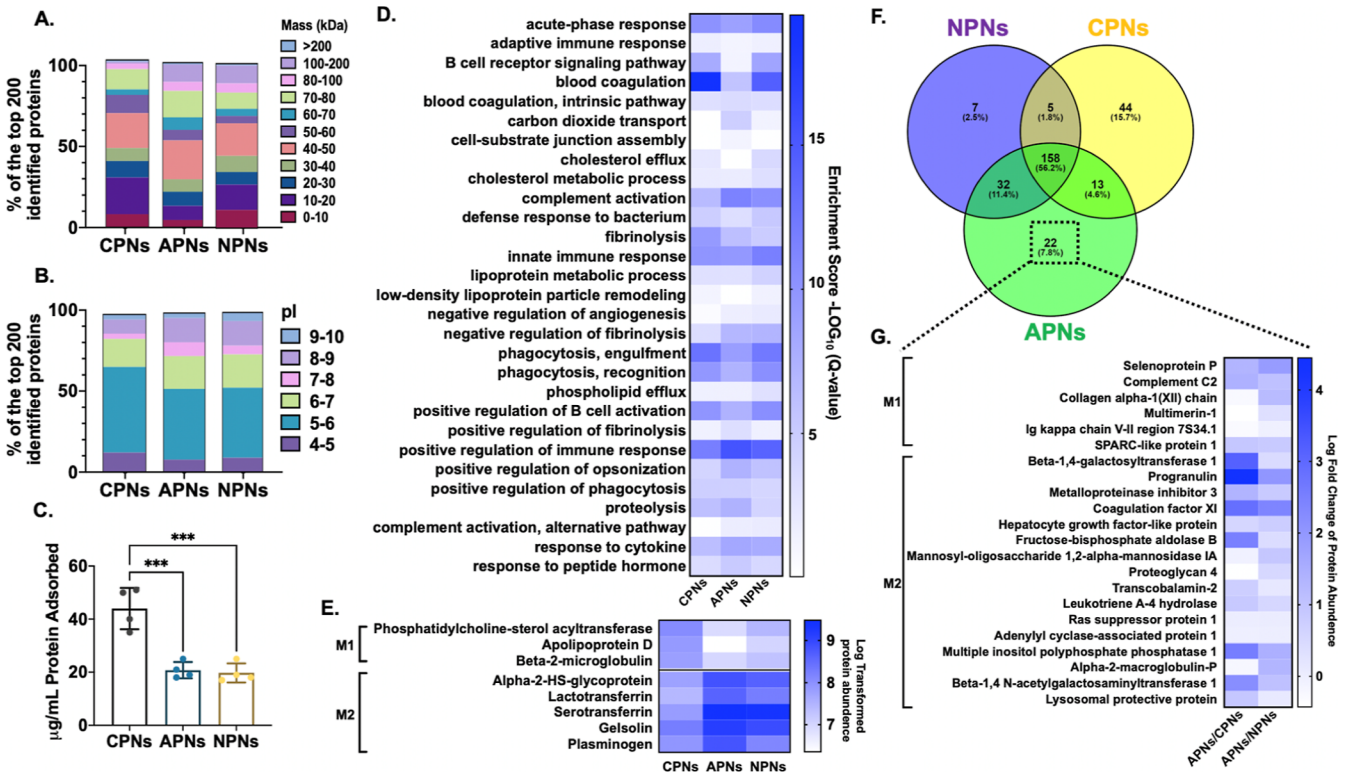

Figure 4. Proteomics from NP protein coronas after exposure to mouse serum suggests charge-specific modulation on macrophage polarization. (A,B) The top 200 corona proteins were distinguished by molecular weight and isoelectric point using UNIPROT and ExPASy. (C) Protein corona amounts were quantified by the BCA assay. (D) Enrichment analysis of the top 200 proteins from each corona. The GO enrichment results were computed using FUNRICH,[57−59] and the GO terms were identified using a published UNIPROT rodent's genome. All listed enrichment scores had a *Q*-value < 0.05. (E) Heatmap of the eight most abundant macrophage polarization-relevant proteins. (F) Venn diagram showing the overlapping identified proteins and distinct proteins from each NP corona. (G) Heatmap of the fold changes of the 22 unique proteins from the anionic NP corona.

taining some pro-inflammatory functions via regulation of the transcription factor IRF4.[50] Although there are limited studies of how macrophages respond to ANPs, APNs decrease M2-like polarization by reducing the CD163 and CD200R expression,[23] which contradicts our findings. This discrepancy might be related to different sources of macrophages (human vs mouse), NP dose, or NP treatment timelines, which highlights the need to comprehensively explore the impact of NP physicochemical properties on macrophage polarization.

In addition to surface charge, NP size also regulates macrophage polarization.[51] There is no definitive agreement on the relationship of size and macrophage phenotype. Some studies report that 5 nm diameter gold NPs (AuNPs) have the greatest inhibition of TNFα compared to AuNPs of 15, 20, and 35 nm diameter.[52,53] Other studies show M2 macrophage markers positively correlate with the NP size.[54,55] Therefore, the impact of NP size on macrophage polarization was tested with 20, 50, and 100 nm APNs (CD bioparticles). After establishing cytocompatibility (Figure S1), macrophage polarization was evaluated using gene expression, flow cytometry, and secreted protein analyses. As reported in Figure 3, all three APNs downregulated macrophage M1 markers, specifically Cxcl11 and Nos2, while upregulating M2 genes (Arg1, CD163, and CD206), with 50 nm NPs exhibiting the greatest effect. Flow cytometry results further confirmed that APNs bias M1-to-M2 macrophage polarization. Indeed, 50 nm APNs exhibited the greatest upregulation in M2 markers while inhibiting M1 markers.

Secreted cytokines were analyzed further to elucidate the impact of NP treatment on macrophage function. Consistent with qPCR and flow cytometry, treatment by all three sizes of APNs decreased pro-inflammatory cytokines (IL1b, IL-2, IL-6, IL-12p70) and increased anti-inflammatory cytokines (IL-4 and IL-10) in M1 macrophages. When comparing the levels of these cytokines, 50 nm NPs reduced the overall number and extent of pro-inflammatory cytokines compared with 20 and 100 nm APNs (Figure 3). Likewise, anti-inflammatory factors induced by 50 nm APNs were the highest. According to these data, 50 nm NPs promote the differentiation of M1-to-M2 more efficiently. In addition to this finding, the effect of NP size on M2 macrophages was tested. 50 nm APNs more effectively inhibit pro-inflammatory factors and promote anti-inflammatory factors. In conclusion, the impact of 50 nm NPs on macrophage M2 polarization is more robust than that of other NP sizes, consistent with other results showing that NP size plays a critical role in NP−cell interactions.[34,56]

Once NPs are introduced to biological fluids, proteins rapidly adsorb and form coronas.[60,61] The protein corona underpins NP−cell interactions, including macrophage polarization.[20,62] NP charge results in different profiles of adsorbed proteins,[28,35,54] which may explain differences in macrophage phenotypic modulation. The protein corona from differently charged NPs was analyzed to investigate this underlying mechanism further. Specifically, CPNs, APNs, and NPNs were exposed to mouse serum for 2 h at 37 °C. The NP and the adsorbed proteins were collected using centrifugation, while

https://doi.org/10.1021/acsami.2c22471
ACS Appl. Mater. Interfaces 2023, 15, 13993−14004

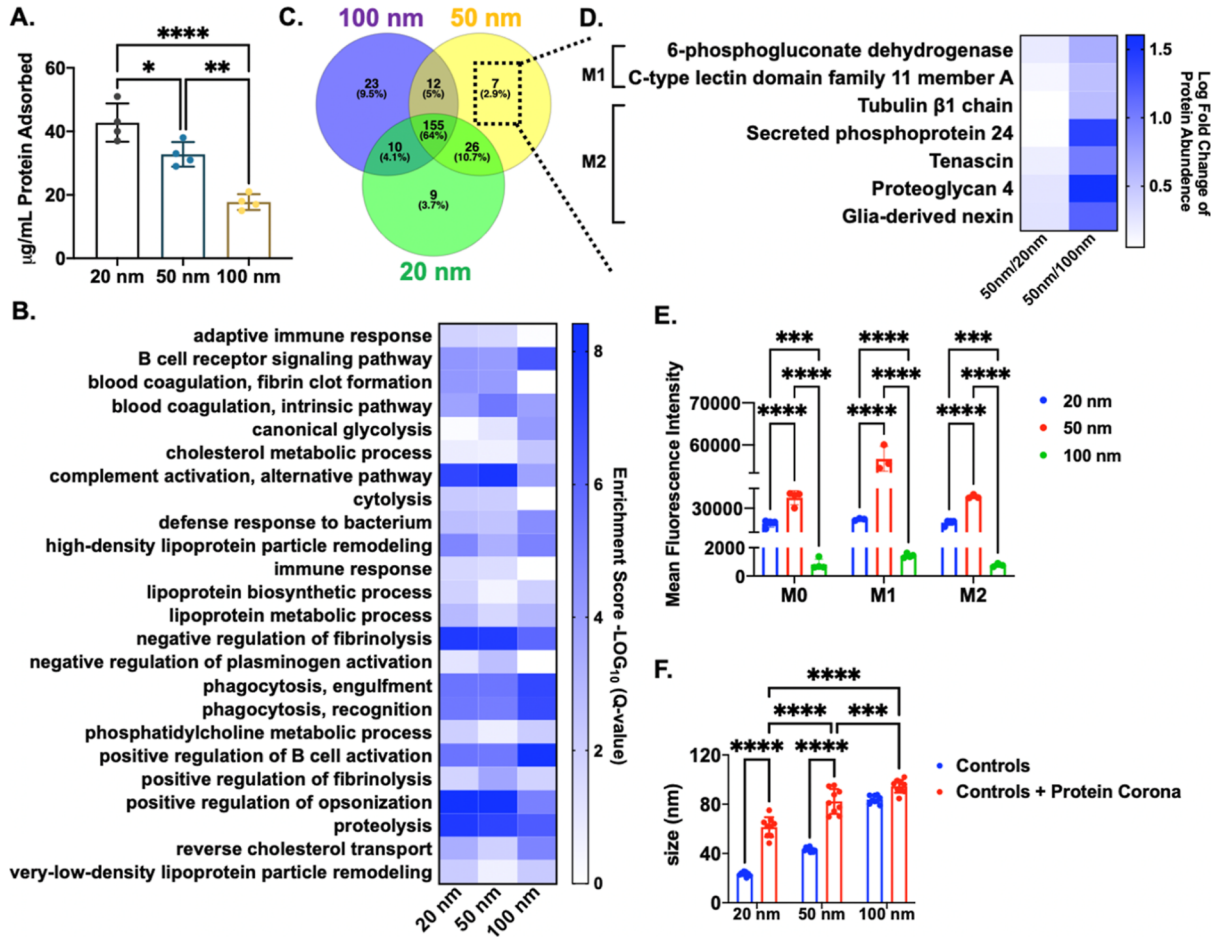

Figure 5. Proteomics from protein coronas of polystyrene NPs with varying sizes suggest that macrophage polarization is dominated by macrophage uptake instead of protein corona. (A) Protein corona amounts were quantified by the BCA assay. (B) Enrichment analysis of the top 200 proteins from each corona. The GO enrichment results were computed using FUNRICH,[57−59] and the GO terms were identified using a published UNIPROT rodent's genome. All listed enrichment scores had a *Q*-value < 0.05. (C) Venn diagram showing the overlapping identified proteins and distinct proteins from each NP corona. (D) Heatmap of the fold changes of the seven unique proteins from the 20 nm NP corona. (E) Macrophage NP uptake analyzed by flow cytometry. (F) DLS of 20, 50, and 100 nm NPs before and after protein adsorption. Data represented as mean ± SD. ***p < 0.001, ****p < 0.0001, determined by two-way ANOVA, multiple comparisons.

the unbound or loosely bound proteins were removed via washing and centrifugation.[27,33] Protein was quantified using the bicinchoninic acid assay (BCA), with CPNs having the greatest overall protein adsorption. Protein adsorption to APNs and NPNs was the same (Figure 4A). While sodium dodecyl sulfate polyacrylamide gel electrophoresis (SDS−PAGE) provides the molecular distribution and the mass of the protein corona, the resolution on the corona profile is relatively low. Therefore, proteomics using liquid chromatography mass spectrometry (LC−MS/MS) was performed to determine the composition of each protein corona quantitatively and qualitatively. A total of 940 proteins were identified within all three protein coronas. The Supporting Information lists the identified proteins. The top 100 or 200 most abundant proteins from each protein corona were selected for analysis. From the protein corona molecular weight composition, APNs had a smaller protein corona mass than the other two coronas (Figure 4B). In contrast, most proteins adsorbed on CPNs had isoelectric points (pI) below 7 compared with the protein coronas from anionic and NPNs (Figure 4C), which is consistent with literature implicating electrostatic interactions' dominating protein adsorption.[28,35] The molecular weight of the protein coronas from all three NPs was similar, with the majority of proteins identified as being 50 kDa or less, consistent with recent findings by Clemments et al.[63]

To further understand how the protein corona formed on cationic, anionic, and neutral polystyrene nanoparticles (CPNs, APNs, and NPNs) affects biological interactions and modulates macrophage polarization, proteomic functional enrichment analysis was performed for all three NP protein coronas using FUNRICH.[57−59] Different immunological responses correlated with the proteins in each corona were discovered by gene ontology (GO) analysis (Figure 4D). A complete list of enriched GO terms, including cellular components, molecular functions, biological processes, protein domains, as well as reactome pathways, is shown in the Supporting Information. According to these analyses, protein coronas from NPs with different charges exhibit distinct biological functions culminating in differential immune processes, similar to prior studies.[31,64] To gain more in-depth knowledge of why NPs with varying charges modulate macrophages, eight macrophage polarization-relevant proteins from the corona were further investigated (Figure 4E). The protein heatmap was plotted based on log-transformed protein abundance, where APNs absorb the greatest M2-relevant proteins and the least M1-associated proteins, which correlates

https://doi.org/10.1021/acsami.2c22471
ACS Appl. Mater. Interfaces 2023, 15, 13993−14004

with the observation that APNs increase M2 and reduce M1 macrophage polarization. M1 and M2-related proteins from the corona are adsorbed to CPNs, which aligns with the simultaneous upregulation of M1 and M2 macrophage phenotype by CPNs. NPNs also adsorb M1 and M2 macrophage-correlated proteins with similar protein level to APNs (Figure 4B). However, no changes in macrophage polarization were observed from NPNs, suggesting that other factors, including possibly the charge itself, may underpin the distinctive macrophage polarization differences.

Venn diagrams were plotted from the top 200 most abundant proteins for each protein corona, of which 158 (56.2%) were shared between anionic, cationic, and neutral NPs (Figure 4F). Nevertheless, each NP had several uniquely adsorbed proteins, suggesting that the NP surface charge plays a role in the composition of protein coronas, consistent with previous reports.[28,35,54] We confirmed that APNs promote macrophages to an M2-like phenotype, and extensive studies have demonstrated that M2 macrophages improve healing.[12,14,20,65−67] Therefore, APNs may be the most promising drug delivery carriers in tissue regeneration applications. However, further investigation is needed to assess whether this charge-dependent macrophage polarization occurs uniformly in other NP systems.

Of the top 200 abundant proteins from the APN protein corona, 22 unique proteins were subsequently explored to determine how they relate to macrophage polarization (Figure 4G). The heatmap was plotted as a log-transformed fold change between anionic to CPNs and anionic to NPNs. Among these 22 proteins, 16 (72.7%) proteins upregulate M2 polarization, while only 6 (27.3%) proteins are implicated in M1 polarization. The abundance of most proteins associated with pro-M2 modulation was much greater than that of those in the other polystyrene NP coronas. Specifically, the fold changes in abundance between APNs and CPNs were 23.5-fold (β-1,4-galactosyltransferase 1), 85.5-fold (Progranulin), 3.9-fold (Metalloproteinase inhibitor 3), 17.2-fold (Coagulation factor XI), 1.8-fold (hepatocyte growth factor-like protein), 12.0-fold (fructose-bisphosphate aldolase B), 2.1-fold (transcobalamin-2), 2.4-fold (leukotriene A-4 hydrolase), onefold (Ras suppressor protein 1), 12.8-fold (multiple inositol polyphosphate phosphatase 1), 9-fold (β-1,4 *N*-acetylglucosaminyltransferase 1), and 2.5-fold (lysosomal protective protein). In addition, several of the pro-M1 proteins from these 22 proteins were less abundant in APN versus CPN coronas, specifically 0.8-fold (collagen a1 (XII) chain), 0.7-fold (multimerin-1), and 0.7-fold (lg kappa VII region 7S34.1). According to these results, since most unique APN corona proteins correlate to M2-like polarization, it is no surprise that macrophages exposed to ANPs polarize preferentially to the M2 phenotype. Although there is a correlation between these unique APN protein profiles and M2-like polarization, one caveat is that the abundance of these proteins is relatively low. For example, when comparing the relative abundance of these unique proteins to albumin, a ubiquitous protein found within the corona, these proteins are 2−3 orders of magnitude lower in abundance (Figure S6). With this consideration, further analysis, including selective protein adsorption from these unique proteins to test individual modulation on macrophage phenotypes, would be beneficial to understand and validate these distinct corona proteins' roles in modulating macrophage polarization. In addition to investigating charge-associated protein corona profiles, mechanistic studies such as exploring the interaction between NP charge and intracellular trafficking will also provide valuable information governing the mechanism of NP charge-dependent macrophage polarization.

Based on the analysis of size, which indicates 50 nm APNs robustly promote M2 polarization (Figure 3), we hypothesized that this phenomenon could be due to varying protein corona identities formed on different-sized polystyrene NPs. To test this hypothesis, protein adsorption was analyzed with 20, 50, and 100 nm APNs. As is shown in Figure 5A, protein adsorption onto 20 nm NPs in the protein corona is the highest, and the absorbed protein decreased with increasing NP sizes. In general, there is an inversely proportional relationship between NP surface energy and size.[34] Of all sizes tested, 20 nm particles have the highest surface energy and greatest protein adsorption, which decreases with increasing size. Our observation that NP surface curvature correlates with protein adsorption is supported by several previous studies.[32,63,68−70] To further explore protein composition, proteomics analysis was performed. The protein compositions from the 20 nm NP corona and 50 nm NP corona are very similar in both molecular weight distribution and pI from the top 200 abundant proteins, while the protein corona of 100 nm NPs has greater 10−20 kDa proteins with pI 5−6 than those in the other two protein coronas (Figure S3).

To further characterize the specific protein content from each corona and correlation to macrophage polarization, proteomic functional enrichment analysis was also performed for these three polystyrene NP coronas using FUNRICH. A complete list of enriched GO terms is shown in the Supporting Information. According to this analysis, coronas from 20 to 50 nm NPs are very similar yet very different from the 100 nm NP corona (Figure 5B). For example, complement activation from the alternative pathway, which is linked to M2 polarization, has greater enrichment in both 20 and 50 nm coronas versus 100 nm NP corona, resulting in 20 and 50 nm NPs to promote M2 macrophage polarization. To further explore the difference between 20, 50, and 100 nm NP protein coronas with respect to M2 polarization, Venn diagrams (Figure 5C) were plotted with the top 200 most abundant proteins, and the seven proteins unique to the 50 nm NP corona were analyzed. As is shown in Figure 5D, although all the M2-related proteins from these 7 proteins have greater abundance in the 50 nm NP corona compared with the 100 nm NP corona, abundance is still very similar to that in the 20 nm NP corona. According to the enrichment analysis and the identification of seven unique proteins from the 50 nm NP corona, protein compositions and proportions are very similar in 20 and 50 nm NP coronas, although the adsorbed protein amounts are different from each other. Based on the compositions, protein coronas from the APN with various sizes were not dominant factors in polarizing macrophages into the M2 phenotype.

To further explore the potential size-dependent impact of APN on macrophage modulation, APN uptake was analyzed via flow cytometry, suggesting that 20 and 50 nm NPs were taken up much more readily than 100 nm NPs (Figure 5E), which might be due to the preferential uptake of smaller NPs by macrophages.[43] Dynamic light scattering was further performed to measure the sizes of different NPs as a function of protein adsorption (Figure 5F). These data suggest that the 80 nm NP−corona complex from 50 nm APN is the most favorable size for macrophage uptake. Furthermore, macrophages took up more 50 nm APN than 20 nm APN, indicating that the higher efficiency in macrophage polarization

https://doi.org/10.1021/acsami.2c22471
ACS Appl. Mater. Interfaces 2023, 15, 13993−14004

modulation with 50 nm APN could be due, in part, to greater NP uptake. In fact, several studies have suggested that NPs of 50 nm diameter are the optimal size for cellular uptake.[71,72] In conclusion, for APNs with a size equal to or less than 100 nm, the impact on macrophage polarization is dominated by the extent of NP uptake rather than protein corona identity. Therefore, NP size can be leveraged to modulate macrophage uptake for expected therapeutic outcomes in applications of delivering APN-based DDSs to macrophages.

Our data show NP physicochemical properties affect protein corona, which correlates to macrophage polarization. First, we show that NP surface charge plays a critical role in macrophage polarization, where cationic nanoparticles potentiate both M1 and M2 macrophage markers while anionic nanoparticles promote M1-to-M2 modulation. Then, consistent with other reports,[20,23,54] proteomics reveals dramatically different protein corona profiles from various charges of NPs. In addition, our thorough analysis of these protein corona profiles enables us to associate these distinct protein profiles with different surface charges to macrophage polarization. Furthermore, we and others showed that the most efficient cellular uptake occurs with 50 nm NPs,[34,54] which can also enhance M2 macrophage polarization. However, in vitro analyses of NP−cell interactions are simplified and do not recapitulate the complexity of the in vivo environment.[73−75] Ongoing studies include in vivo analysis to further understand protein corona's role in NP−macrophage interactions. The findings regarding NP-modulated macrophage polarization are of great value to the clinical translation of nanotechnologies since the macrophage polarization state is linked to disease progression. Therefore, macrophage polarization can be targeted and modulated when designing NP DDSs. For example, since TAMs show greater M2 macrophage polarization, which promotes tumor cell proliferation and invasion,[10,11] NP DDSs that inhibit M2 macrophage modulation can be used as a critical parameter for anti-tumor DDS design. Additionally, M2 macrophages improve fracture healing.[14] In this case, relevant DDSs that promote M2 macrophage polarization can be utilized to enhance healing outcomes. Nevertheless, macrophage modulation is dynamic, with gradation between myriad phenotypes that vary temporally.[9,65,66] Therefore, time-dependent studies are necessary to discover macrophage−polarization-related temporal effects. Finally, in vivo nanotoxicological studies should also be considered to assess undesired effects and ensure the safe translation of NP-based DDSs from bench to bedside.[76] Altogether, investigating NP-mediated macrophage polarization and uncovering underlying mechanisms provide valuable information and guide DDS engineering for clinical use.

CONCLUSIONS

Our analysis identified physicochemical properties of NPs, such as charge and size, as having distinct impacts on macrophage polarization, which was then confirmed with the other NPs more relevant to drug delivery. Specifically, cationic nanoparticles promote both M1 and M2 macrophage polarization, whereas anionic nanoparticles bias M2-like macrophage modulation. Macrophages are actively involved in many diseases, where various macrophage polarization statuses and types exert significant differences in disease progression. Therefore, based on our findings, physicochemical properties of NP DDSs should be carefully considered to avoid unwanted macrophage polarization. Due to distinct NP protein corona formation, it is critical to be able to characterize the protein coronas from various NPs and, ultimately, explore their correlation with NP-mediated macrophage polarization. Our proteomics analysis of protein coronas revealed distinct protein corona patterns from different physicochemical properties of NPs, which underpins the differential impact of NPs on macrophage polarization. Furthermore, future studies are warranted to comprehensively investigate the impact of other physicochemical properties, such as material, shape, and surface modification, etc., on the protein corona and its relationship to macrophage modulation.[77,84] Altogether, this work can serve as a foundation for investigating the underlying mechanism of NP-mediated macrophage polarization.

METHODS

Polymer Synthesis, NP Self-Assembly, and Characterization. Amphiphilic diblock copolymers of poly(styrene-*alt*-maleic anhydride)-*b*-poly(styrene) (PSMA-*b*-PS) were synthesized via reversible addition−fragmentation chain transfer (RAFT) polymerization, as described previously.[6,46,47,78,79] PSMA-*b*-PS copolymers were then self-assembled into NPs via solvent exchange with a hydrophobic core (PS) and a hydrophilic shell (PSMA).[6,46,47,78,79] DMAEMA NPs, consisting of a pH-responsive core and cationic corona, were self-assembled from poly(dimethylmethacrylate)-*b*-poly(dimethylaminoethyl methacrylate-*co*-butyl methacrylate-*co*-propylacrylic acid) or p(DMAEMA)-*b*-p(DMAEMA-*co*-BMA-PAA) also synthesized via RAFT, as described previously.[45,80] For PEG-PS copolymers, PS-COOH was first synthesized via RAFT, followed by carbodiimide chemistry for conjugation of PEG to PS-COOH in an organic solvent.[80,81] Polymer molecular weights were determined with gel permeation chromatography (GPC). NP size and surface charge were measured using DLS (Malvern Instruments, Worcestershire, UK), where the polymer concentration is 0.1 mg/mL.

Cell Culture and Macrophage Polarization. BMDMs were harvested from female 6−8 weeks old Balb/c mice (Jackson Laboratory). Briefly, femurs and tibias were harvested, bones were rinsed with cold PBS, and the flushed marrows were filtered through a 70 mm cell strainer. Following centrifugation, the cell pellets were lysed with red blood cell lysis buffer (5 mL for 1 min on ice), and subsequently, the RBC lysis buffer was neutralized with 15 mL of high-glucose Dulbecco's modified Eagle medium (DMEM, Gibco) supplemented with 10% fetal bovine serum (FBS) and 100 units/mL penicillin−streptomycin (Gibco), followed by centrifugation at 1100 rpm for 5 min. After resuspending the cells gently in 15 mL of DMEM containing a macrophage colony-stimulating factor (M-CSF, 25 ng/mL), they were plated into a T-75 flask and grown for 24 h. At this point, if any adherent stromal cells and resident macrophages adhered to the flask, then all non-adherent cells were transferred to a new plate or flask for further differentiation. At day 7, cells were ready for M1 polarization with 50 ng/mL of lipopolysaccharide (LPS) and 25 ng/mL of interferon-γ (INF-γ) and M2 polarization with 20 ng/mL of interleukin-4 (IL-4).

Flow Cytometry. M0, M1, and M2-polarized macrophages were treated with different NPs for 1 day. Cells were collected for cell surface marker analysis using flow cytometry. The gating strategy of flow cytometry is shown in Figure S5. Specifically, bone marrow-derived macrophages were gated for F4/80+CD45+Ly6C-Ly6G-cells to achieve a relatively pure population, and M1 and M2 phenotypes were identified as MHCII+CD38+ and CD206+CD163+, respectively, from the previously gated bone marrow-derived macrophage population. The impact of NPs on M1 and M2 polarization was analyzed by the percentage of M1 and M2 markers, normalized by untreated groups.

Quantitative Real-Time PCR. At 24 h, cells treated with NPs and the untreated group were collected for quantifying gene expression levels. Briefly, RNA was extracted from cell pellets lysed with TRK lysis buffer (Bio-Rad) containing 2-mercaptoethanol (1% v/v). After determining the quantity and quality of extracted RNA via Cytation 5

https://doi.org/10.1021/acsami.2c22471
ACS Appl. Mater. Interfaces 2023, 15, 13993−14004

(Biotek) by the A260/280 ratio, cDNA was synthesized using the iScript cDNA Synthesis Kit (Bio-Rad), and PCR was performed by the PowerUp SYBR Green Master Mix Assay (Applied Biosystems) to investigate the impact of polarization on a gene expression level. Primer sequences are listed in Table S1.

Macrophage Function Evaluation via Cytokine Release. After gene expression and a cell surface marker test, macrophage function was further evaluated by Luminex (Eve Technologies) by testing both pro-inflammatory and anti-inflammatory cytokines released in the cell culture media. Specifically, these cytokines include granulocyte−macrophage colony-stimulating factor (GM-CSF), IFNγ, IL-1β, IL-2, IL-4, IL-6, IL-10, IL-12p70, monocyte chemoattractant protein-1 (MCP-1), and tumor necrosis factor α (TNF-α).

Protein Corona Formation and Gel Electrophoresis for Proteomics. 50 mL of NPs (50 mg/mL) were incubated in 50 mL of mouse serum for 2 h at 37 °C. Unbound proteins were washed away using 3 times of centrifugation at 30,000 rpm at 4 °C with 1× PBS for 40 min each. After that, the pellet was resuspended in 100 mL of 2 wt % SDS in 1× PBS. 16 mL of these NP protein coronas were mixed with 4 mL of Lane Marker Reducing Sample buffer (Thermo) and incubated for 5 min at 95 °C. The resulting mixtures and a protein ladder were loaded into a 4−20% mini-PROTEAN TGX Precast protein gel (Bio-Rad) at 100 V for 15 min to get a 1 cm-long band. The gels were washed 3 times for 5 min each in 200 mL of ddH_2O to remove SDS, which will interfere with the following staining. 100 mL of Bio-Safe Coomassie stain was used to stain the bands with gentle shaking overnight. The gels were finally rinsed extensively in ddH_2O after staining to further reduce background. The gels were then submitted for proteomics analysis.

Sample Preparation for Proteomics. The regions of interior in the gel were first cut into 1 mm cubes, de-stained, and then reduced and alkylated with dithiothreitol (DTT) and iodoacetamide (IAA), respectively (Sigma). Acetonitrile was used to dehydrate the gel fragments. Trypsin (Promega) aliquots were reconstituted to 10 ng/μL in 50 mM ammonium bicarbonate and added until just covering the dehydrated gel pieces. The gel pieces were submerged completely in ammonium bicarbonate after 30 min at room temperature, and then the gel was placed at 37 °C overnight. The following day, peptides were extracted by adding 50% acetonitrile and 0.1% trifluoroacetic acid (TFA), followed by drying down in a CentriVap concentrator (Labconco). Using handmade C18 spin columns, peptides were desalted before being dried one more time and reconstituting in 0.1% TFA.

Mass Spectrometry. The Easy nLC-1200 HPLC (Thermo Fisher) was coupled to a Fusion Lumos Tribrid mass spectrometer, and 1.8 μm beads (Sepax) were used to introduce peptides into the column from each fraction (Thermo Fisher). While solvent B contained 0.1% formic acid in 80% acetonitrile, solvent A contained 0.1% formic acid in water. A Nanospray Flex source running at 2 kV was used to inject ions into the mass spectrometer. The gradient started at 3% B and held for 2 min. It then increased to 10% B over 6 min, to 38% B over 35 min, to 90% B in 5 min, and was held for 3 min. It then ramped back down to the beginning conditions in 2 min and stabilized for 7 min, making for a total run time of 60 min. A data-independent mode was used to operate the Fusion Lumos. With a resolution of 60,000 at 200 m/z, an AGC target of 4×10^5, and a maximum injection duration of 50 ms, the entire MS1 scan was performed. A staggered windowing approach of 20 m/z with 10 m/z overlaps was used to monitor precursor ions. For instance, the final window fragmented ions between 980 and 1000 m/z, while the first cycle fragmented precursor ions between 400 and 420 m/z, 420 and 440 m/z, etc. The following cycle fragmented precursor ions between 390 and 410 m/z, then 410−430 m/z, etc., with ions between 990 and 1010 m/z serving as the cycle's ultimate fragmentation. The number of MS2 scans in each cycle was 30, and the collection of fragment ions ranged from 200 to 2000 m/z. By applying a collision energy of 33%, precursor ions were broken up by higher-energy C-trap dissociation (HCD). With a resolution of 15,000, an AGC target of 4×10^5, and a maximum injection time of 23 ms, MS2 images were amassed in the Orbitrap.

Data Analysis. DIA-NN version 1.8.1 (https://github.com/vdemichev/DIA-NN)[82] was used to process raw data. Data analysis for all experiments was done in DIA-library-free NN's analysis mode. The mouse UniProt database (UP000000589 10090, downloaded 4/7/2021) with "deep learning-based spectra and RT prediction" enabled was used to annotate the library. For Ox(M), the maximum number of variable modifications was set to 1, the maximum number of missed cleavages was set to 1, the peptide length range was set to 7−30, the precursor charge range was set to 2−3, the precursor m/z range was set to 400−1000, and the fragment m/z range was set to 200−2000. The protein inferences were set to "Genes," and "Heuristic protein inference" was disabled. The quantification was performed in "Robust LC (high precision)" mode. The software automatically establishes the scan window size, MS1 and MS2 mass tolerances, and other parameters. Subsequently, the posterior error probability (50%) and the library protein group (1% each) Q-values were used to filter the precursors. The amount of peptides quantified in each protein group was tallied using the MaxLFQ algorithm as implemented in the DIA-NN R package (https://github.com/vdemichev/diann-rpackage) and the DiannReportGenerator Package (https://github.com/kswovick/DIANN-Report-Generator).[83].

■ ASSOCIATED CONTENT

Supporting Information

The Supporting Information is available free of charge at https://pubs.acs.org/doi/10.1021/acsami.2c22471.

Additional experimental details, methods, and additional figures for NMR, GPC, DLS, and biocompatibility results et al. (PDF)

Proteomics raw data and list of proteins from various NP coronas (XLSX)

■ AUTHOR INFORMATION

Corresponding Author

Danielle S. W. Benoit − *Department of Biomedical Engineering, University of Rochester, Rochester, New York 14623, United States; Center for Musculoskeletal Research, University of Rochester Medical Center, Rochester, New York 14623, United States; Department of Chemical Engineering and Materials Science Program, University of Rochester, Rochester, New York 14623, United States; Phil and Penny Knight Campus for Accelerating Scientific Impact, Department of Bioengineering, University of Oregon, Eugene, Oregon 97403, United States;* orcid.org/0000-0001-7137-8164; Email: dbenoit@uoregon.edu

Authors

Baixue Xiao − *Department of Biomedical Engineering, University of Rochester, Rochester, New York 14623, United States; Center for Musculoskeletal Research, University of Rochester Medical Center, Rochester, New York 14623, United States;* orcid.org/0000-0001-8337-8401

Yuxuan Liu − *Materials Science Program, University of Rochester, Rochester, New York 14623, United States*

Indika Chandrasiri − *Department of Biomedical Engineering, University of Rochester, Rochester, New York 14623, United States; Center for Musculoskeletal Research, University of Rochester Medical Center, Rochester, New York 14623, United States*

Clyde Overby − *Department of Biomedical Engineering, University of Rochester, Rochester, New York 14623, United States; Center for Musculoskeletal Research, University of Rochester Medical Center, Rochester, New York 14623, United States*

Complete contact information is available at:
https://pubs.acs.org/10.1021/acsami.2c22471

Author Contributions

The manuscript was written through contributions of all authors. All authors have given approval to the final version of the manuscript Funding

Funding

This work was supported by grants from the National Science Foundation (NSF) (CBET1450987 and DMR2103553); National Institutes of Health (NIH) (R01 AR064200, R01 AR056696, P30 AR06955, R21 AR081063 (to DB) and S10 OD030302); Orthopaedic Research and Education Foundation Grant 20-072 (to DB), Orthopaedic Trauma Association Grant 6272 (to DB), and the University of Rochester Medical Center Department of Orthopaedics Goldstein Award (to DB).

Notes

The authors declare no competing financial interest.

ACKNOWLEDGMENTS

The authors also wish to thank Kevin Welle, Matthew Cochran, Celia Soto, Ming Yan, Emily Quarato, and Jared Mereness for their assistance.

ABBREVIATIONS

MPS, mononuclear phagocyte system
NP, nanoparticle
CPNs, cationic polystyrene nanoparticles
APNs, anionic polystyrene nanoparticles
NPNs, neutral polystyrene nanoparticles
BMDMs, bone marrow-derived monocytes
Cxcl11, CXC motif chemokine ligand 11
Nos2, nitric oxide synthase 2
IL1β, interleukin 1β
Arg1, arginase 1
MHCII, major histocompatibility complex class II
CCL17, C−C motif chemokine ligand 17
GAPDH, glyceraldehyde-3-phosphate dehydrogenase
DDSs, drug delivery systems
TAM, tumor-associated macrophage
M-CSF, macrophage colony-stimulating factor
GM-CSF, granulocyte-macrophage colony-stimulating factor
IFNγ, interferon gamma
IL-6, interleukin 6
IL-12p70, interleukin 12
MCP-1, monocyte chemoattractant protein-1
TNFα, tumor necrosis factor α
IL-4, interleukin 4
IL-10, interleukin 10
DMAEMA-NP, poly(dimethylaminoethyl methacrylate)-*b*-poly(dimethylaminoethyl methacrylate-*co*-butyl methacrylate-*co*-propylacrylic acid) nanoparticle
PSMA-PS NP, poly(styrene-*alt*-maleic anhydride)-poly(styrene)
PEG-PS NPs, poly(ethylene glycol)-*b*-poly(styrene)
GPC, gel permeation chromatography
NMR, nuclear magnetic resonance
DLS, dynamic light scattering
TLR4, toll-like receptor 4 signaling
AuNPs, gold nanoparticles
GO, gene ontology
pI, isoelectric point
BCA, bicinchoninic acid assay
LC−MS/MS, liquid chromatography−mass spectrometry

REFERENCES

(1) Mitchell, M. J.; Billingsley, M. M.; Haley, R. M.; Wechsler, M. E.; Peppas, N. A.; Langer, R. Engineering Precision Nanoparticles for Drug Delivery. *Nat. Rev. Drug Discovery* **2021**, *20*, 101−124.
(2) Shen, J.; Lu, Z.; Wang, J.; Zhang, T.; Yang, J.; Li, Y.; Liu, G.; Zhang, X. Advances of Nanoparticles for Leukemia Treatment. *ACS Biomater. Sci. Eng.* **2020**, *6*, 6478−6489.
(3) Zhang, R. X.; Li, J.; Zhang, T.; Amini, M. A.; He, C.; Lu, B.; Ahmed, T.; Lip, H.; Rauth, A. M.; Wu, X. Y. Importance of Integrating Nanotechnology with Pharmacology and Physiology for Innovative Drug Delivery and Therapy—An Illustration with Firsthand Examples. *Acta Pharmacol. Sin.* **2018**, *39*, 825−844.
(4) Xiao, J.; Zhu, Y.; Huddleston, S.; Li, P.; Xiao, B.; Farha, O. K.; Ameer, G. A. Copper Metal-Organic Framework Nanoparticles Stabilized with Folic Acid Improve Wound Healing in Diabetes. *ACS Nano* **2018**, *12*, 1023−1032.
(5) Yi, S.; Zhang, X.; Sangji, H.; Liu, Y.; Allen, S. D.; Xiao, B.; Bobbala, S.; Braverman, C. L.; Cai, L.; Hecker, P. I.; DeBerge, M.; Thorp, E. B.; Temel, R. E.; Stupp, S. I.; Scott, E. A. Surface Engineered Polymersomes for Enhanced Modulation of Dendritic Cells during Cardiovascular Immunotherapy. *Adv. Funct. Mater.* **2019**, *29*, 1904399.
(6) Ackun-Farmmer, M. A.; Xiao, B.; Newman, M. R.; Benoit, D. S. W. Macrophage Depletion Increases Target Specificity of Bone-targeted Nanoparticles. *J. Biomed. Mater. Res. A* **2022**, *110*, 229.
(7) Medrano-Bosch, M.; Moreno-Lanceta, A.; Melgar-Lesmes, P. Nanoparticles to Target and Treat Macrophages: The Ockham's Concept? *Pharmaceutics* **2021**, *13*, 1340.
(8) Gustafson, H. H.; Holt-Casper, D.; Grainger, D. W.; Ghandehari, H. Nanoparticle Uptake: The Phagocyte Problem. *Nano Today* **2015**, *10*, 487−510.
(9) Niu, Y.; Wang, Z.; Shi, Y.; Dong, L.; Wang, C. Modulating Macrophage Activities to Promote Endogenous Bone Regeneration: Biological Mechanisms and Engineering Approaches. *Bioact. Mater.* **2021**, *6*, 244−261.
(10) Reichel, D.; Tripathi, M.; Perez, J. M. Biological Effects of Nanoparticles on Macrophage Polarization in the Tumor Microenvironment. *Nanotheranostics* **2019**, *3*, 66−88.
(11) Galletti, G.; Scielzo, C.; Barbaglio, F.; Rodriguez, T. V.; Riba, M.; Lazarevic, D.; Cittaro, D.; Simonetti, G.; Ranghetti, P.; Scarfò, L.; Ponzoni, M.; Rocchi, M.; Corti, A.; Anselmo, A.; van Rooijen, N.; Klein, C.; Ries, C. H.; Ghia, P.; De Palma, M.; Caligaris-Cappio, F.; Bertilaccio, M. T. S. Targeting Macrophages Sensitizes Chronic Lymphocytic Leukemia to Apoptosis and Inhibits Disease Progression. *Cell Rep.* **2016**, *14*, 1748−1760.
(12) Jain, S.; Tran, T. H.; Amiji, M. Macrophage Repolarization with Targeted Alginate Nanoparticles Containing IL-10 Plasmid DNA for the Treatment of Experimental Arthritis. *Biomaterials* **2015**, *61*, 162−177.
(13) Clark, D.; Brazina, S.; Yang, F.; Hu, D.; Hsieh, C. L.; Niemi, E. C.; Miclau, T.; Nakamura, M. C.; Marcucio, R. Age-related Changes to Macrophages are Detrimental to Fracture Healing in Mice. *Aging Cell* **2020**, *19*, No. e13112.
(14) Löffler, J.; Sass, F. A.; Filter, S.; Rose, A.; Ellinghaus, A.; Duda, G. N.; Dienelt, A. Compromised Bone Healing in Aged Rats Is Associated With Impaired M2 Macrophage Function. *Front. Immunol.* **2019**, *10*, 2443.
(15) Yang, X.; Feng, W.; Wang, R.; Yang, F.; Wang, L.; Chen, S.; Ru, Y.; Cheng, T.; Zheng, G. Repolarizing Heterogeneous Leukemia-associated Macrophages with More M1 Characteristics Eliminates their Pro-leukemic Effects. *Oncoimmunology* **2018**, *7*, No. e1412910.
(16) Rahal, O. M.; Wolfe, A. R.; Mandal, P. K.; Larson, R.; Tin, S.; Jimenez, C.; Zhang, D.; Horton, J.; Reuben, J. M.; McMurray, J. S.;

Woodward, W. A. Blocking Interleukin (IL)4- and IL13-Mediated Phosphorylation of STAT6 (Tyr641) Decreases M2 Polarization of Macrophages and Protects Against Macrophage-Mediated Radioresistance of Inflammatory Breast Cancer. *Int. J. Radiat. Oncol., Biol., Phys.* **2018**, *100*, 1034−1043.
(17) Smirnova, T.; Spertini, C.; Spertini, O. CSF1R Inhibition Combined with GM-CSF Reprograms Macrophages and Disrupts Protumoral Interplays with AML Cells. *Cancers* **2021**, *13*, 5289.
(18) Li, J.; Kaneda, M. M.; Ma, J.; Li, M.; Shepard, R. M.; Patel, K.; Koga, T.; Sarver, A.; Furnari, F.; Xu, B.; Dhawan, S.; Ning, J.; Zhu, H.; Wu, A.; You, G.; Jiang, T.; Venteicher, A. S.; Rich, J. N.; Glass, C. K.; Varner, J. A.; Chen, C. C. PI3Kγ inhibition suppresses microglia/TAM accumulation in glioblastoma microenvironment to promote exceptional temozolomide response. *Proc. Natl. Acad. Sci. U.S.A.* **2021**, *118*, No. e2009290118.
(19) Zheng, Y.; Yang, J.; Qian, J.; Qiu, P.; Hanabuchi, S.; Lu, Y.; Wang, Z.; Liu, Z.; Li, H.; He, J.; Lin, P.; Weber, D.; Davis, R. E.; Kwak, L.; Cai, Z.; Yi, Q. PSGL-1/selectin and ICAM-1/CD18 Interactions Are Involved in Macrophage-induced Drug Resistance in Myeloma. *Leukemia* **2013**, *27*, 702−710.
(20) Miao, X.; Leng, X.; Zhang, Q. The Current State of Nanoparticle-Induced Macrophage Polarization and Reprogramming Research. *Int. J. Mol. Sci.* **2017**, *18*, 336.
(21) Wang, D.; Bratlie, K. M. Influence of Polymer Chemistry on Cytokine Secretion from Polarized Macrophages. *ACS Biomater. Sci. Eng.* **2015**, *1*, 166−174.
(22) Bygd, H. C.; Forsmark, K. D.; Bratlie, K. M. Altering in vivo macrophage responses with modified polymer properties. *Biomaterials* **2015**, *56*, 187−197.
(23) Fuchs, A. K.; Syrovets, T.; Haas, K. A.; Loos, C.; Musyanovych, A.; Mailänder, V.; Landfester, K.; Simmet, T. Carboxyl- and Amino-functionalized Polystyrene Nanoparticles Differentially Affect the Polarization Profile of M1 and M2 Macrophage Subsets. *Biomaterials* **2016**, *85*, 78−87.
(24) Docter, D.; Westmeier, M.; Markiewicz, S.; Stolte, S. K.; Knauer, R. H.; Stauber, R. H. The Nanoparticle Biomolecule Corona: Lessons Learned − Challenge Accepted? *Chem. Soc. Rev.* **2015**, *44*, 6094−6121.
(25) Lynch, I.; Dawson, K. A. Protein−Nanoparticle Interactions. *Nano Today* **2008**, *3*, 40−47.
(26) Lynch, I.; Cedervall, T.; Lundqvist, M.; Cabaleiro-Lago, C.; Linse, S.; Dawson, K. A. The Nanoparticle−protein Complex as a Biological Entity; A Complex Aluids and Surface Science Challenge for the 21st Century. *Adv. Colloid Interface Sci.* **2007**, *134*−*135*, 167−174.
(27) Cedervall, T.; Lynch, I.; Foy, M.; Berggård, T.; Donnelly, S. C.; Cagney, G.; Linse, S.; Dawson, K. A. Detailed Identification of Plasma Proteins Adsorbed on Copolymer Nanoparticles. *Angew. Chem., Int. Ed. Engl.* **2007**, *46*, 5754−5756.
(28) Lee, H. Effects of Nanoparticle Electrostatics and Protein-Protein Interactions on Corona Formation: Conformation and Hydrodynamics. *Small* **2020**, *16*, No. e1906598.
(29) Debayle, M.; Balloul, E.; Dembele, F.; Xu, X.; Hanafi, M.; Ribot, F.; Monzel, C.; Coppey, M.; Fragola, A.; Dahan, M.; Pons, T.; Lequeux, N. Zwitterionic Polymer Ligands: an Ideal Surface Coating to Totally Suppress Protein-nanoparticle Corona Formation? *Biomaterials* **2019**, *219*, 119357.
(30) Zeuthen, C. M.; Shahrokhtash, A.; Sutherland, D. S. Nanoparticle Adsorption on Antifouling Polymer Brushes. *Langmuir* **2019**, *35*, 14879−14889.
(31) Tenzer, S.; Docter, D.; Kuharev, J.; Musyanovych, A.; Fetz, V.; Hecht, R.; Schlenk, F.; Fischer, D.; Kiouptsi, K.; Reinhardt, C.; Landfester, K.; Schild, H.; Maskos, M.; Knauer, S. K.; Stauber, R. H. Rapid Formation of Plasma Protein Corona Critically Affects Nanoparticle Pathophysiology. *Nat. Nanotechnol.* **2013**, *8*, 772−781.
(32) Mahmoudi, M.; Lynch, I.; Ejtehadi, M. R.; Monopoli, M. P.; Bombelli, F. B.; Laurent, S. Protein-nanoparticle Interactions: Opportunities and Challenges. *Chem. Rev.* **2011**, *111*, 5610−5637.
(33) Cedervall, T.; Lynch, I.; Lindman, S.; Berggård, T.; Thulin, E.; Nilsson, H.; Dawson, K. A.; Linse, S. Understanding the Nanoparticle-protein Corona using Methods to Quantify Exchange Rates and Affinities of Proteins for Nanoparticles. *Proc. Natl. Acad. Sci. U.S.A.* **2007**, *104*, 2050−2055.
(34) Lundqvist, M.; Stigler, J.; Elia, G.; Lynch, I.; Cedervall, T.; Dawson, K. A. Nanoparticle Size and Surface Properties Determine the Protein Corona with Possible Implications for Biological Impacts. *Proc. Natl. Acad. Sci. U.S.A.* **2008**, *105*, 14265−14270.
(35) Pustulka, S. M.; Ling, K.; Pish, S. L.; Champion, J. A. Protein Nanoparticle Charge and Hydrophobicity Govern Protein Corona and Macrophage Uptake. *ACS Appl. Mater. Interfaces* **2020**, *12*, 48284−48295.
(36) Saha, K.; Rahimi, M.; Yazdani, M.; Kim, S. T.; Moyano, D. F.; Hou, S.; Das, R.; Mout, R.; Rezaee, F.; Mahmoudi, M.; Rotello, V. M. Regulation of Mac Recognition through the Interplay of Nanoparticle Surface Functionality and Protein Corona. *ACS Nano* **2016**, *10*, 4421−4430.
(37) Walkey, C. D.; Olsen, J. B.; Guo, H.; Emili, A.; Chan, W. C. Nanoparticle Size and Surface Chemistry Determine Serum Protein Adsorption and Macrophage Uptake. *J. Am. Chem. Soc.* **2012**, *134*, 2139−2147.
(38) Wilson, C. J.; Clegg, R. E.; Leavesley, D. I.; Pearcy, M. J. Mediation of Biomaterial-cell Interactions by Adsorbed Proteins: a Review. *Tissue Eng.* **2005**, *11*, 1−18.
(39) Klein, J. Probing the Interactions of Proteins and Nanoparticles. *Proc. Natl. Acad. Sci. U.S.A.* **2007**, *104*, 2029−2030.
(40) Walczyk, D.; Bombelli, M. P.; Monopoli, I.; Lynch, K. A.; Dawson, K. A. What the Cell "Sees" in Bionanoscience. *J. Am. Chem. Soc.* **2010**, *132*, 5761−5768.
(41) Yang, H.; Lu, S.; Wang, S.; Liu, L.; Zhu, B.; Yu, S.; Yang, S.; Chang, J. Evolution of the Protein Corona Affects Macrophage Polarization. *Int. J. Biol. Macromol.* **2021**, *191*, 192−200.
(42) Lunov, O.; Syrovets, T.; Loos, C.; Beil, J.; Delacher, M.; Tron, K.; Nienhaus, G. U.; Musyanovych, A.; Mailänder, V.; Landfester, K.; Simmet, T. Differential Uptake of Functionalized Polystyrene Nanoparticles by Human Macrophages and a Monocytic Cell Line. *ACS Nano* **2011**, *5*, 1657−1669.
(43) Lesniak, A.; Campbell, A.; Monopoli, M. P.; Lynch, I.; Salvati, A.; Dawson, K. A. Serum Heat Inactivation Affects Protein Corona Composition and Nanoparticle Uptake. *Biomaterials* **2010**, *31*, 9511−9518.
(44) Barnes, C. A.; Elsaesser, A.; Arkusz, J.; Smok, A.; Palus, J.; Leśniak, A.; Salvati, A.; Hanrahan, J. P.; Jong, W. H.; Dziubałtowska, E.; Stępnik, M.; Rydzyński, K.; McKerr, G.; Lynch, I.; Dawson, K. A.; Howard, C. V. Reproducible Comet Assay of Amorphous Silica Nanoparticles Detects No Genotoxicity. *Nano Lett.* **2008**, *8*, 3069−3074.
(45) Roncari Rocha, G.; Sims, K. R., Jr.; Xiao, B.; Klein, M. I.; Benoit, D. S. W. Nanoparticle Carrier Co-delivery of Complementary Antibiofilm Drugs Abrogates Dual Species Cariogenic Biofilm Formation In vitro. *J. Oral Microbiol.* **2022**, *14*, 1997230.
(46) Baranello, M. P.; Bauer, L.; Benoit, D. S. Poly(styrene-alt-maleic anhydride)-based Diblock Copolymer Micelles Exhibit Versatile Hydrophobic Drug Loading, Drug-dependent Release, and Internalization by Multidrug Resistant Ovarian Cancer Cells. *Biomacromolecules* **2014**, *15*, 2629−2641.
(47) Wang, Y.; Newman, M. R.; Ackun-Farmmer, M.; Baranello, M. P.; Sheu, T. J.; Puzas, J. E.; Benoit, D. S. W. Fracture-Targeted Delivery of Beta-Catenin Agonists via Peptide-Functionalized Nanoparticles Augments Fracture Healing. *ACS Nano* **2017**, *11*, 9445−9458.
(48) Lunov, O.; Syrovets, T.; Loos, C.; Nienhaus, G. U.; Mailänder, V.; Landfester, K.; Rouis, M.; Simmet, T. Amino-functionalized Polystyrene Nanoparticles Activate the NLRP3 Inflammasome in Human Macrophages. *ACS Nano* **2011**, *5*, 9648−9657.
(49) Huang, Z.; Yang, Y.; Jiang, Y.; Shao, J.; Sun, X.; Chen, J.; Dong, L.; Zhang, J. Anti-tumor Immune Responses of Tumor-associated

https://doi.org/10.1021/acsami.2c22471
ACS Appl. Mater. Interfaces 2023, 15, 13993−14004

Macrophages via Toll-like Receptor 4 Triggered by Cationic Polymers. *Biomaterials* **2013**, *34*, 746−755.
(50) Pena, O. M.; Afacan, N.; Pistolic, J.; Chen, C.; Madera, L.; Falsafi, R.; Fjell, C. D.; Hancock, R. E. Synthetic Cationic Peptide IDR-1018 Modulates Human Macrophage Differentiation. *PLoS One* **2013**, *8*, No. e52449.
(51) Ma, J.; Liu, R.; Wang, X.; Liu, Q.; Chen, Y.; Valle, R. P.; Zuo, Y. Y.; Xia, T.; Liu, S. Crucial Role of Lateral Size for Graphene Oxide in Activating Macrophages and Stimulating Pro-inflammatory Responses in Cells and Animals. *ACS Nano* **2015**, *9*, 10498−10515.
(52) Sumbayev, V. V.; Yasinska, I. M.; Garcia, C. P.; Gilliland, D.; Lall, G. S.; Gibbs, B. F.; Bonsall, D. R.; Varani, L.; Rossi, F.; Calzolai, L. Gold Nanoparticles Downregulate Interleukin-1beta-induced Pro-inflammatory Responses. *Small* **2013**, *9*, 472−477.
(53) Tsai, C. Y.; Lu, S. L.; Hu, C. W.; Yeh, C. S.; Lee, G. B.; Lei, H. Y. Size-dependent Attenuation of TLR9 Signaling by Gold Nanoparticles in Macrophages. *J. Immunol.* **2012**, *188*, 68−76.
(54) Chen, X.; Gao, C. Influences of Size and Surface Coating of Gold Nanoparticles on Inflammatory Activation of Macrophages. *Colloids Surf., B* **2017**, *160*, 372−380.
(55) MacParland, S. A.; Tsoi, K. M.; Ouyang, B.; Ma, X. Z.; Manuel, J.; Fawaz, A.; Ostrowski, M. A.; Alman, B. A.; Zilman, A.; Chan, W. C.; McGilvray, I. D. Phenotype Determines Nanoparticle Uptake by Human Macrophages from Liver and Blood. *ACS Nano* **2017**, *11*, 2428−2443.
(56) Jiang, Y.; Huo, S.; Mizuhara, T.; Das, R.; Lee, Y. W.; Hou, S.; Moyano, D. F.; Duncan, B.; Liang, X. J.; Rotello, V. M. The Interplay of Size and Surface Functionality on the Cellular Uptake of Sub-10 nm Gold Nanoparticles. *ACS Nano* **2015**, *9*, 9986−9993.
(57) Pathan, M.; Keerthikumar, S.; Chisanga, D.; Alessandro, R.; Ang, C. S.; Askenase, P.; Batagov, A. O.; Benito-Martin, A.; Camussi, G.; Clayton, A.; Collino, F.; Di Vizio, D.; Falcon-Perez, J. M.; Fonseca, P.; Fonseka, P.; Fontana, S.; Gho, Y. S.; Hendrix, A.; Hoen, E. N.; Iraci, N.; Kastaniegaard, K.; Kislinger, T.; Kowal, J.; Kurochkin, I. V.; Leonardi, T.; Liang, Y.; Llorente, A.; Lunavat, T. R.; Maji, S.; Monteleone, F.; Øverbye, A.; Panaretakis, T.; Patel, T.; Peinado, H.; Pluchino, S.; Principe, S.; Ronquist, G.; Royo, F.; Sahoo, S.; Spinelli, C.; Stensballe, A.; Théry, C.; Herwijnen, M. J. C.; Wauben, M.; Welton, J. L.; Zhao, K.; Mathivanan, S. A Novel Community Driven Software for Functional Enrichment Analysis of Extracellular Vesicles Data. *J. Extracell. Vesicles* **2017**, *6*, 1321455.
(58) Pathan, M.; Keerthikumar, S.; Ang, C. S.; Gangoda, L.; Quek, C. Y.; Williamson, N. A.; Mouradov, D.; Sieber, O. M.; Simpson, R. J.; Salim, A.; Bacic, A.; Hill, A. F.; Stroud, D. A.; Ryan, M. T.; Agbinya, J. I.; Mariadason, J. M.; Burgess, A. W.; Mathivanan, S. FunRich: An Open Access Standalone Functional Enrichment and Interaction Network Analysis Tool. *Proteomics* **2015**, *15*, 2597−2601.
(59) Benito-Martin, A.; Peinado, H. FunRich proteomics software analysis, let the fun begin! *Proteomics* **2015**, *15*, 2555−2556.
(60) Gray, J. J. The Interaction of Proteins with Solid Surfaces. *Curr. Opin. Struct. Biol.* **2004**, *14*, 110−115.
(61) Kane, R. S.; Stroock, A. D. Nanobiotechnology: Protein-nanomaterial Interactions. *Biotechnol. Prog.* **2007**, *23*, 316−319.
(62) Monopoli, M. P.; Åberg, C.; Salvati, A.; Dawson, K. A. Biomolecular Coronas Provide the Biological Identity of Nanosized Materials. *Nat. Nanotechnol.* **2012**, *7*, 779−786.
(63) Clemments, A. M.; Botella, P.; Landry, C. C. Protein Adsorption From Biofluids on Silica Nanoparticles: Corona Analysis as a Function of Particle Diameter and Porosity. *ACS Appl. Mater. Interfaces* **2015**, *7*, 21682−21689.
(64) Palmieri, V.; Caracciolo, G. Tuning the Immune System by Nanoparticle-biomolecular Corona. *Nanoscale Adv.* **2022**, *4*, 3300−3308.
(65) Wasnik, S.; Rundle, C. H.; Baylink, D. J.; Yazdi, M. S.; Carreon, E. E.; Xu, Y.; Qin, X.; Lau, K. W.; Tang, X. 1,25-Dihydroxyvitamin D Suppresses M1 Macrophages and Promotes M2 Differentiation at Bone Injury Sites. *JCI Insight* **2018**, *3*, No. e98773.
(66) Zhang, R.; Liang, Y.; Wei, S. M2 Macrophages are Closely Associated With Accelerated Clavicle Fracture Healing in Patients with Traumatic Brain Injury: a Retrospective Cohort Study. *J. Orthop. Surg. Res.* **2018**, *13*, 213.
(67) Loi, F.; Córdova, L. A.; Zhang, R.; Pajarinen, J.; Lin, T. H.; Goodman, S. B.; Yao, Z. The Effects of Immunomodulation by Macrophage Subsets on Ssteogenesis In vitro. *Stem Cell Res. Ther.* **2016**, *7*, 15.
(68) Roach, P.; Farrar, D.; Perry, C. C. Surface Tailoring for Controlled Protein Adsorption: Effect of Topography at the Nanometer Scale and Chemistry. *J. Am. Chem. Soc.* **2006**, *128*, 3939−3945.
(69) Shang, W.; Nuffer, J. H.; Muñiz-Papandrea, V. A.; Colón, W.; Siegel, R. W.; Dordick, J. S. Cytochrome C on Silica Nanoparticles: Influence of Nanoparticle Size on Protein Structure, Stability, and Activity. *Small* **2009**, *5*, 470−476.
(70) Vollath, D.; Fischer, F. D.; Holec, D. Surface Energy of Nanoparticles-Influence of Particle Size and Structure. *Beilstein J. Nanotechnol.* **2018**, *9*, 2265−2276.
(71) Zhang, S.; Li, J.; Lykotrafitis, G.; Bao, G.; Suresh, S. Size-Dependent Endocytosis of Nanoparticles. *Adv. Mater.* **2009**, *21*, 419−424.
(72) Lu, F.; Wu, S. H.; Hung, Y.; Mou, C. Y. Size Effect on Cell uptake in Well-suspended, Uniform Mesoporous Silica Nanoparticles. *Small* **2009**, *5*, 1408−1413.
(73) Mahmoudi, M.; Bertrand, N.; Zope, H.; Farokhzad, O. C. Emerging Understanding of the Protein Corona at the Nano-bio Interfaces. *Nano Today* **2016**, *11*, 817−832.
(74) Safavi-Sohi, R.; Maghari, S.; Raoufi, M.; Jalali, S. A.; Hajipour, M. J.; Ghassempour, A.; Mahmoudi, M. Bypassing Protein Corona Issue on Active Targeting: Zwitterionic Coatings Dictate Specific Interactions of Targeting Moieties and Cell Receptors. *ACS Appl. Mater. Interfaces* **2016**, *8*, 22808−22818.
(75) Mahmoudi, M.; Sheibani, S.; Milani, A. S.; Rezaee, F.; Gauberti, M.; Dinarvand, R.; Vali, H. Crucial Role of the Protein Corona for the Specific Targeting of Nanoparticles. *Nanomedicine* **2015**, *10*, 215−226.
(76) Domingues, C.; Santos, A.; Alvarez-Lorenzo, C.; Concheiro, A.; Jarak, I.; Veiga, F.; Barbosa, I.; Dourado, M.; Figueiras, A. Where Is Nano Today and Where Is It Headed? A Review of Nanomedicine and the Dilemma of Nanotoxicology. *ACS Nano* **2022**, *16*, 9994−10041.
(77) Lynch, I.; Salvati, K. A.; Dawson, K. A. Protein-nanoparticle Interactions: What Does the Cell See? *Nat. Nanotechnol.* **2009**, *4*, 546−547.
(78) Ackun-Farmmer, M. A.; Soto, C. A.; Lesch, M. L.; Byun, D.; Yang, L.; Calvi, L. M.; Benoit, D. S. W.; Frisch, B. J. Reduction of Leukemic Burden via Bone-targeted Nanoparticle Delivery of an Inhibitor of C-chemokine (C-C motif) Ligand 3 (CCL3) Signaling. *FASEB J.* **2021**, *35*, No. e21402.
(79) Newman, M. R.; Russell, S. G.; Schmitt, C. S.; Marozas, I. A.; Sheu, T. J.; Puzas, J. E.; Benoit, D. S. W. Multivalent Presentation of Peptide Targeting Groups Alters Polymer Biodistribution to Target Tissues. *Biomacromolecules* **2018**, *19*, 71−84.
(80) Chen, B. G.; Gao, J.; Kops, W.; Batsberg, W. Preparation of Polystyrene-poly (ethylene glycol) Diblock Copolymer by "Living" Free Radical Polymerisation. *Polymer* **1998**, *39*, 911−915.
(81) Chandrasiri, Y. L.; Liu, Y.; Adjei-Sowah, E.; Xiao, B.; Benoit, D. S. W. Reproducible and controlled peptide functionalization of polymeric nanoparticles. *Front. Biomater. Sci.* **2022**, *1*, 1003172.
(82) Demichev, V.; Messner, C. B.; Vernardis, S. I.; Lilley, K. S.; Ralser, M. DIA-NN: neural networks and interference correction enable deep proteome coverage in high throughput. *Nat. Methods* **2020**, *17*, 41−44.
(83) Cox, J.; Hein, M. Y.; Luber, C. A.; Paron, I.; Nagaraj, N.; Mann, M. Accurate Proteome-wide Label-free Quantification by Delayed Normalization and Maximal Peptide Ratio Extraction, Termed MaxLFQ. *Mol. Cell. Proteomics* **2014**, *13*, 2513−2526.
(84) Lynch, I.; Dawson, K. A.; Linse, S. Detecting Cryptic Epitopes Created by Nanoparticles. *Sci. STKE* **2006**, *2006*, pe14.

https://doi.org/10.1021/acsami.2c22471
ACS Appl. Mater. Interfaces 2023, 15, 13993−14004